Annals of Nuclear Medicine Vol. 21, No. 1, 1–8, 2007

PET kinetic analysis —Pitfalls and a solution for the Logan plot

Yuichi KIMURA,* Mika NAGANAWA,*,** Miho SHIDAHARA,*** Yoko IKOMA*** and Hiroshi WATABE****

*Positron Medical Center, Tokyo Metropolitan Institute of Gerontology
**Japanese Society for the Promotion of Science
***Molecular Imaging Center, National Institute of Radiological Sciences
****Department of Investigative Radiology, National Cardiovascular Center Research Institute

The Logan plot is a widely used algorithm for the quantitative analysis of neuroreceptors using PET because it is easy to use and simple to implement. The Logan plot is also suitable for receptor imaging because its algorithm is fast. However, use of the Logan plot, and interpretation of the formed receptor images should be regarded with caution, because noise in PET data causes bias in the Logan plot estimates. In this paper, we describe the basic concept of the Logan plot in detail and introduce three algorithms for the Logan plot. By comparing these algorithms, we demonstrate the pitfalls of the Logan plot and discuss the solution.

Key words: PET, kinetic analysis, Logan plot, receptor imaging

I. INTRODUCTION

PET enables us to quantify various functionalities of living tissue such as receptor density and the activity of enzymes. Ordinarily, to derive the functionalities, a nonlinear optimization algorithm is applied to measured PET data of a time history of radioactivity in tissues (tissue time-activity curve, tTAC; in Bq/m*l*) and in arterial plasma (plasma time-activity curve, pTAC; in Bq/m*l*) to analyze the compartmental models parametrically.[1] Applying the algorithm to every voxel but not to a tTAC averaged in a region of interest (ROI) allows the imaging of some functionalities of living tissues. However, the algorithm suffers from some problems that make it unsuitable for the kinetic analysis in a voxel-by-voxel manner, such as physiologically unacceptable parameter estimates, dependency to an initial guess[2] and slow calculation time.

The Logan plot[3] is an algorithm used widely for receptor imaging because of its simple mathematical implementation and fast computation. The Logan plot can be realized as a line estimation,[4] making it stable and very fast. Thus, the Logan plot is preferred for voxel-by-voxel kinetic analysis. However, the estimates suffer seriously from noise in the tTAC.

In this paper, we describe the theoretical background of the Logan plot. We mention the pitfalls of the Logan plot, a bias in estimated receptor quantity, and discuss the solution.

II. THEORY OF THE LOGAN PLOT

The Logan plot is derived by integrating a set of differential equations describing the behavior of an administered ligand in target tissues. (1) represents the basics of Logan plot in which the two quantities have a linear relationship, and the slope of this relationship and the *y*-intercept are denoted as α and β: ratios of an integrated tTAC and tTAC, and an integrated pTAC and tTAC. (2) shows the slope and *y*-intercept for the two-compartment model, α_{2C} and β_{2C}, and α_{3C} and β_{3C} in (3) represent those for a three-compartment model. The detailed derivation is available in the appendix.

$$\underbrace{\frac{\int_0^t C(u)du}{C(t)}}_{Y} = \alpha \underbrace{\frac{\int_0^t C_p(u)du}{C(t)}}_{X} + \beta \qquad (1)$$

Received December 18, 2006, revision accepted December 18, 2006.

For reprint contact: Yuichi Kimura, Ph.D., Positron Medical Center, Tokyo Metropolitan Institute of Gerontology, 1–1, Naka, Itabashi, Tokyo, 173–0022, JAPAN.
E-mail: ukimura@ieee.org

$$\begin{cases} \alpha_{2C} = (1 - B_v)\dfrac{K_1}{k_2} + B_v \\ \beta_{2C} = -\dfrac{1 - B_v}{k_2}\dfrac{1}{(1 - B_v) + B_v \dfrac{C_p(t)}{\tilde{C(t)}}} \end{cases} \quad (2)$$

$$\begin{cases} \alpha_{3C} = (1 - B_v)\dfrac{K_1}{k_2}\left(1 + \dfrac{k_3}{k_4}\right) + B_v \\ \beta_{3C} = -\dfrac{1 - B_v}{k_2 k_4}\left\{(k_3 + k_4)\dfrac{\tilde{C(t)}}{C(t)} + k_2 \dfrac{\tilde{C_b(t)}}{C(t)}\right\} \end{cases} \quad (3)$$

$C(t)$,$C_p(t)$, and B_v denote tTAC, pTAC, and blood volume [m*l*/m*l*], respectively. $\tilde{C(t)}$ is a true tTAC, which does not contain the activities originating from blood vessels in a voxel or ROI; this means B_v. K_1 to k_4 are kinetic parameters of the administered radioligand in tissues that were proposed originally by Mintun[5] and extended to the general compartmental model for receptor study by Koeppe.[6] To summarize, K_1 represents the transportation rate of a ligand from capillary to tissues [m*l*/min/g], and k_2 is the clearance rate back to the venous system [1/min]. k_3 and k_4 are the association and disassociation rates of the ligand to and from the specific binding sites [1/min]. More descriptions can be seen in an other article in this survey series.[1]

The ratio of the following quantities reaches a constant equilibrium state: C_p and $\tilde{C}$ for the two-compartment model; and the measured tTAC and the activity in tissues; and the measured tTAC and the activity originating from unbound ligand in the tissues for the three-compartment model. Under these conditions, the *y*-intercepts of β become constant against time, and a linear relation is established in (1).

If B_v is small enough in (2) or (3), the slope of the Logan plot corresponds to K_1/k_2 for the two-compartment model and to $(K_1/k_2)(1 + k_3/k_4)$ for the three-compartment model. These quantities are named the total distribution volume, DV_t, and they are the substituted measures for receptor densities. Note that the slope derived from the Logan plot is biased from the true DV_t because B_v is contained in the term of the slope.

III. MERITS OF THE LOGAN PLOT

The Logan plot has three merits: independence from a kinetic model, stable algorithm, and fast computational time.

First, the Logan plot is applicable in both two- and three-compartment models. This means that the configuration of the compartmental model does not affect the usability of the Logan plot, although it should be determined before the model estimation in an ordinary kinetic analysis using nonlinear estimation.

Second, the Logan plot is realized as a line estimation.[4] Because the line estimation algorithm has closed forms, we can compute the slope and *y*-intercept directly using pTAC and tTAC. In contrast, in a nonlinear model estimation, the model parameters are sought iteratively, as described below.

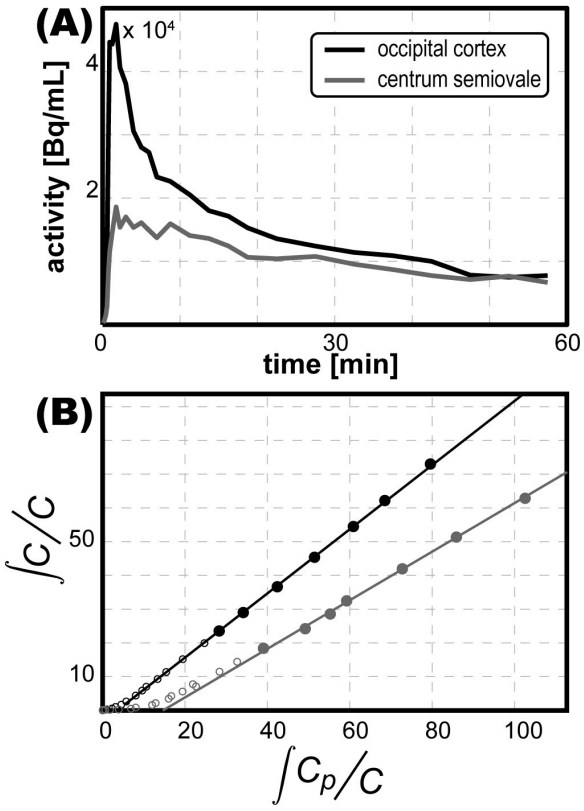

Fig. 1 Typical Logan plot of [^{11}C]TMSX, an antagonist of adenosine A_{2A} receptors. The upper panel (A) shows the tTACs, and the lower panel (B) demonstrates the corresponding Logan plots. The plot of the centrum semiovale and the occipital cortex are shown in black and gray, respectively, and the filled symbols show the data applied to the line estimation. The receptor density is greater in the occipital cortex than in the centrum semiovale, and the slopes reflect this difference. In these data, the DV_t of the centrum semiovale and occipital cortex were 0.95 and 0.72 [m*l*/g], respectively.

In the nonlinear model estimation, the estimation begins from given parameters as initial values. The next best estimates are tried and found based on the local shape of a cost function to be minimized that is usually the root mean square between the measured and predicted tTAC. This step is repeated until no further improvements are found in the estimates or the cost function. Finding the precise shape of the cost function is complicated because the relationship between the model parameters and the cost function is not straightforward, and this causes multiple local optima in the cost function. An ordinary nonlinear optimization algorithm such as the Lovenberg-Marquardt method[7] and Nelder-Mead Simplex method[8] can find only the local optimal point, which is not necessarily globally minimal and can vary depending on the given initial guess.

As mentioned above, the nonlinear model estimation is

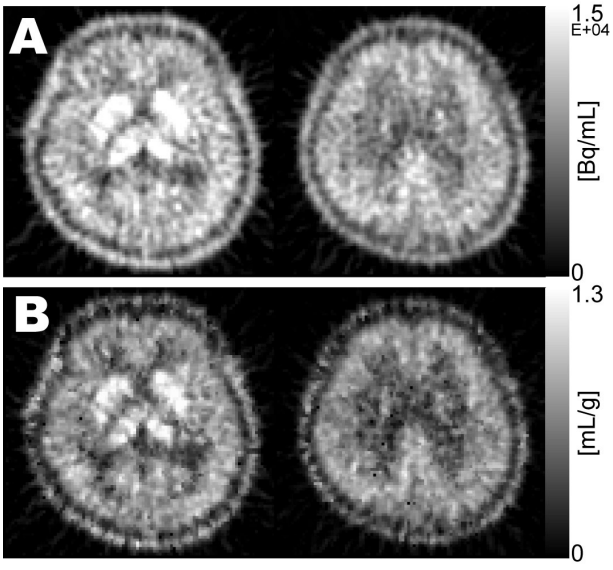

Fig. 2 Static images in (A) and images of total distribution volume in (B) computed by the Logan plot for [^{11}C]TMSX, a radioligand for the adenosine A_{2A} receptors.

affected by the initial values. In the case of bad noise statistics in tTAC, the results of the estimation sometimes change with the given initial values or can sometimes converge to physiologically unacceptable values such as negatives or values larger than 1.0.[2] Fortunately, the Logan plot assures reasonable estimates.

Third, the Logan plot has fast computation. The iterative implementation of a nonlinear model estimation demands extensive computation, and convolution operations are required to calculate the predicted tTAC, which complicates the computation. In a typical Logan plot implementation, the computation time is only 2 [μsec/voxel], but an ordinary compartment model analysis requires 1 [sec/voxel] if the standard desktop computer with Windows XP^{TM} is used.

IV. EXAMPLE OF THE LOGAN PLOT

An example of the Logan plot is shown in Figure 1 and has been derived from [^{11}C]TMSX, an antagonist of the adenosine A_{2A} receptor.[9] Figure 1-(A) shows the tTACs derived from the centrum semiovale and occipital cortex. The corresponding Logan plots are displayed in (B), which shows superimposed estimated lines and the data used in the line estimation as filled plots. The tTACs decrease in the delayed phase, a typical pattern observed with reversible ligands. In the Logan plot, a linear relation is also found 20 minutes after administration. Because of its physiological aspect, the centrum semiovale has negligible A_{2A} binding sites.[9] Therefore, the slope of the plot is smaller in the centrum semiovale (= 0.72) than in the occipital lobe (= 0.95).

Figure 2 illustrates one benefit of the Logan plot in

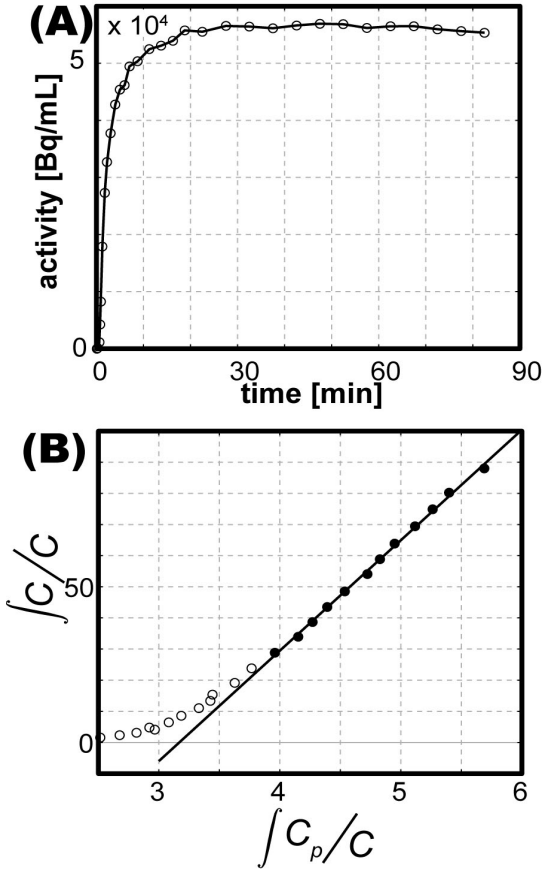

Fig. 3 The Logan plot applied to [^{11}C]SA4503, an antagonist of sigma$_1$ receptors. The upper panel (A) shows a typical tTAC derived from the temporal cortex of a normal subject. The lower panel (B) illustrates the corresponding Logan plot where the filled plots represent the data for the line estimation. Although the waveform seems to depart from the shape expected for reversible binding, a linear relationship is apparent in (B).

receptor imaging. Panel (A) shows the summed images, and (B) shows images of DV_t computed by the Logan plot where the left and right images present the slices including the striatum and centrum semiovale, respectively. The DV_t images have better contrast than the summed images because they represent the density of the A_{2A} receptors. The centrum semiovale appears darker than the cerebral cortices in (B) and this is more obvious in (B) than in (A). Also, the striatum is visualized more clearly in (B) than in (A).

Another example is shown in Figure 3, which represents the calculations for [^{11}C]SA4503,[10] a radioligand for the sigma$_1$ receptors. Because of the high affinity of [^{11}C]SA4503 to the binding sites, the tTAC does not demonstrate reversible behavior and its value does not decrease when compared with Figure 1-(A). However, the Logan plot shown in Figure 3-(B) has a fairly linear relationship 30 minutes after administration of the antagonist. As Logan remarked, the condition for the Logan plot is rather easy to establish.[11]

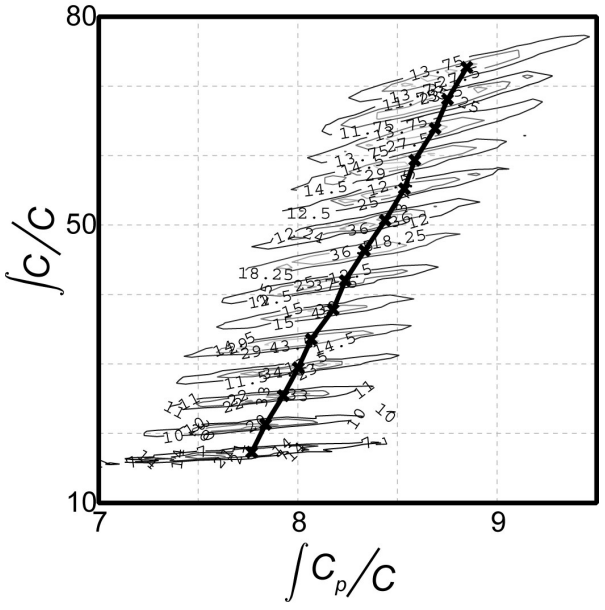

Fig. 4 Statistical distribution in the Logan plot. 5000 realizations of voxel-based tTACs were mimicked, and their statistical fluctuation of each plot in the Logan plot was displayed as two-dimensional histograms in the form of a contour plot.

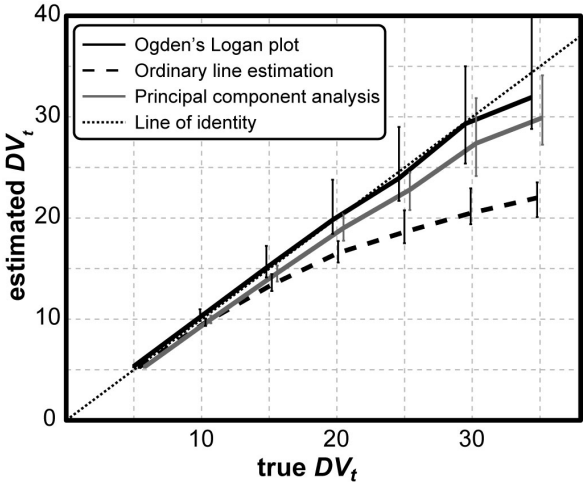

Fig. 5 Comparison of the estimation performance of the Logan plot using an ordinary regression line estimation (solid black line), PC-based line estimation (solid gray line), and the Ogden's Logan plot (dashed black line). DV_t was varied from 5 to 35, and 100 tTACs were simulated with contamination by noise found in a voxel-based tTAC for each DV_t. Then, the estimated DV_t was computed using the three algorithms. Medians and the 75% and 25% quintiles are plotted using a bar plot. A line of identity is indicated by a dotted line. For clear visualization, the abscissa is slightly shifted to prevent overlapping.

The Logan plot is thought to be a powerful tool for receptor imaging in PET.

V. ALGORITHM

Because the implementation of an algorithm influences the performance of the Logan plot, we discuss three algorithms in this section. The first two algorithms are related to a line estimation based on the original idea in the Logan plot: an ordinary regression line estimation (OLE) and a line estimation using a principal component, PC.[12] The third algorithm estimates tTAC using the relationship available in the Logan plot in a manner of a likelihood estimation, Ogden's Logan plot, OP.[13]

V-A. Logan plot based on regression line estimation

An easy choice is OLE in which the sum of the squared differences is minimized between an estimated line and given data measured along a line perpendicular to the abscissa. This choice is a mistake for imaging, however, because OLE assumes that the noise of the independent variables, named X, is much smaller than that of the dependent variables, Y, and if this assumption is not established, the absolute value of the estimated slope by OLE becomes smaller than the true value.[14] For the Logan plot, as reported in,[15] the noise in tTAC causes a negative bias in DV_t estimates, and the magnitude of the bias depends on the noise level. Large noise causes a large underestimation of DV_t.

This situation is serious in the formation of parametric images because voxel-based tTACs are highly tainted by noise. According to (1), both X and Y contain a voxel-based tTAC of $C(t)$ in the denominators. The noise in a voxel-based tTAC is large because of the small amount of radioactivity in a voxel, and the independent variable is contaminated by the noise in tTAC. The exact fluctuation caused by noise in voxel-based tTACs is demonstrated in Figure 4 where 5,000 realizations of tTACs containing voxel-based noise were generated and the Logan plots were carried out. Their distributions are shown as two-dimensional histograms in the form of a contour plot. The deviation in the abscissa cannot be ignored, and the deviation between X and Y is correlated when X and Y are large.

V-B. Logan plot based on principal component

A better choice is to apply PC,[12] in which the minimized distances are measured perpendicular to an estimated line. (4) is the operational equation for PC:

$$\begin{cases} S_{xx} = \sum_i x_i^2,\ S_{yy} = \sum_i y_i^2,\ S_{xy} = \sum_i x_i y_i \\ \bar{x} = \frac{1}{N}\sum_i x_i,\ \bar{y} = \frac{1}{N}\sum_i y_i \\ \hat{\alpha} = \frac{(S_{xx} - S_{yy}) + \sqrt{(S_{xx} - S_{yy})^2 + 4(S_{xy})^2}}{2S_{xy}} \\ \hat{\beta} = \bar{y} - \alpha\hat{\bar{x}} \end{cases} \quad (4)$$

where $\hat{\alpha}$ and $\hat{\beta}$ represent the estimated slope and y-intercept, respectively, x_i and y_i are the ith measured set of

data, and N is the number of frames during the period in which the Logan plot is applied. Because PC considers the existence of noise in both the independent and dependent variables, better performance can be expected.

V-C. Likelihood approach for Logan plot

Another advanced approach than PC was proposed by Ogden.[13] In OP, an anticipated tTAC, $\hat{C}$, is computed based on the relationship in the Logan plot in a recurring equation:

$$\hat{C_i}(\alpha,\beta) = \frac{\sum_{j=1}^{i-1} C_j \hat{W}_j + \frac{1}{8}\hat{C_{i-1}} W_{i-1} - \alpha \int_0^{t_i} C_p(u)du}{\beta - \frac{3}{8}W_{i-1}} \quad (5)$$

where C_i and W_i are the measured tTAC at the ith frame and it frame duration, respectively. (5) is derived from the relationship in the Logan plot. The tTAC at the ith frame appears as the second term in the numerator is introduced using a trapezoidal integral.

The slope and y-intercept of the Logan plot are reckoned through likelihood estimation by fitting the measured tTAC to the anticipated one:

$$[\alpha\beta\hat{]} = \underset{\alpha,\beta}{\operatorname{argmin}} \sum_i^N \left\{ C_i - \hat{C_i}(\alpha,\beta) \right\}^2. \quad (6)$$

In OP, the estimation process is performed in a time domain, and OP is free from the problems caused by the noise of independent variables in the case of OLE.

VI. PITFALLS AND SOLUTION

To demonstrate the pitfalls of the Logan plot related to the noise in tTAC, the performance of the three algorithms and a dependency of estimated DV_t on the noise are shown in Figure 5 and Figure 6, respectively, which were derived from a set of simulations that considered a voxel-based parameter estimation.

Simulated tTACs were computed using a clinically measured pTAC in a [^{11}C]SA4503 dynamic study with the defined kinetic parameters for each simulation. The noise was then added to the level observed in voxel-based tTACs. The noise was assumed to have a Gaussian distribution whose variance was proportional to the true tTAC and whose mean was zero. To derive the descriptive statistics, 100 tTACs were realized.

The total performance of DV_t estimation is illustrated in Figure 5. In this simulation, K_1, DV (= K_1/k_2), and k_3 were set to their typical values of 0.1, 0.49, and 0.45, respectively, and DV_t was varied from 5 to 35. This simulation produced a range of k_4 between 0.006 and 0.049. The median and 25% and 75% quartiles are indicated as a bar plot.

OLE introduced incorrect DV_t estimates because the medians were much lower than the true value. PC also showed a small underestimation, which tended to worsen in larger DV_t. In contrast, OP gave almost true DV_t. OLE showed the smallest estimation deviation of the three algorithms; PC produced an intermediate estimation deviation, and OP produced the largest estimation deviation.

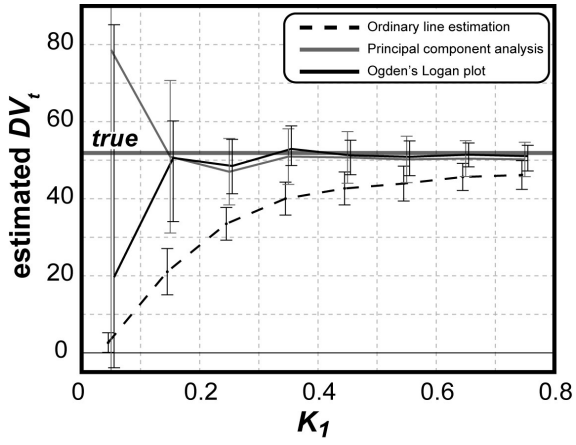

Fig. 6 Dependency of DV_t estimates on K_1. tTACs were simulated with DV_t fixed at 53 and with K_1 varying. Noise was added to the level observed in a voxel-based tTAC. The plotted DV_t were estimated using the three algorithms. The means and standard deviations derived from 100 realizations are shown. The three algorithms of the Logan plot based on an ordinary regression line estimation, PC-based line estimation, and the Ogden's Logan plot are shown.

The noise dependency of DV_t estimates on K_1 is shown in Figure 6. K_1 was varied within a physiologically feasible range between 0.05 and 0.8 while DV_t was fixed at 53, a typical value of [^{11}C]SA4503 for normal subjects.[16]

Although ideally no dependencies should be observed, the estimates using OLE correlated with K_1, with a low K_1 making the estimates lower. That is why the amplitude of tTAC tends to be governed mainly by K_1 when the tTAC decreases slowly, as in the case of [^{11}C]SA4503. The noise level becomes large when the amplitude is small. A small K_1 causes a low amplitude and large noise level in tTAC, and leads to underestimating the estimated DV_t. This dependency leads to erroneously enhanced contrast of a DV_t image; that is, the contrast of a DV_t image is enhanced because of the mathematical problems in the estimation algorithm, and the enhanced image matches the preconceived image the people want to see. The DV_t image with OLE causes misinterpretation of the spatial distribution of the neuroreceptors, and the PC and the OP are not correlated with K_1.

One may inspect the differences between the three algorithms in Figure 7. These DV_t images were computed from the same PET data of [^{11}C]SA4503 administered to a young male subject. The slice includes the basal ganglia. Note that the displayed ranges obtained using the OLE and PC algorithms differ from that obtained using OP. DV_t in the images using OLE is smaller than those of the other algorithms; the PC image produced an intermediate value, and OP had the largest DV_t. This tendency

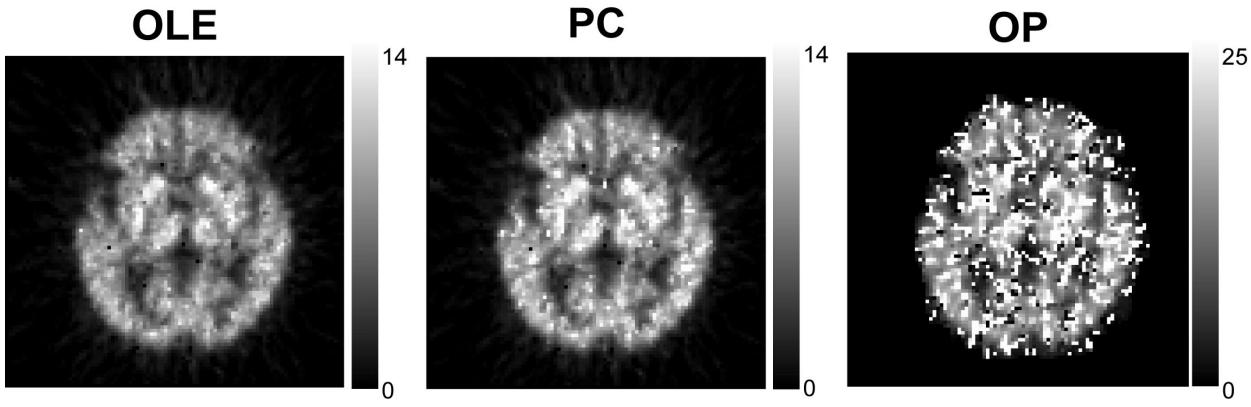

Fig. 7 DV_t images using the three algorithms: an ordinary line estimation of OLE, a PC-based line estimation of PC, and the Ogden's Logan plot of OP. The images were made from the same original PET data using [^{11}C]SA4503, a radioligand for the sigma$_1$ receptors.

corresponds to the simulation results as shown in Figure 5. Although the contrast between brain structures was maintained in all algorithms, the image quality was poor in OP.

The computation time was noticeable. In our implementation using MATLAB™ R14 (MathWorks, MA, USA), the computational times per slice were 0.11 [msec] for OLE and PC, and 9.7 [min] for OP using a Linux machine equipped with a 3.2 [GHz] Pentium-IV processor. OLE and PC are fast to run because they have closed forms to compute DV_t. In contrast, OP requires a nonlinear optimization algorithm, and it demands computation because the implementation is iterative.

As a consequence, PC is the optimal choice for receptor imaging using the Logan plot. OP is also attractive because it is free from the problem in a line estimation caused by the noise in an independent variable. Further studies are expected to make the algorithm faster and to fix the problems identified.

VII. OTHER TOPICS

Other related topics to the Logan plot are summarized.

The first issue is the omission of arterial blood sampling. The Logan plot requires pTAC to calculate DV_t, as shown in (1). For clinical considerations, omission of arterial blood sampling is welcome because arterial blood sampling requires the placement of a catheter into the brachial artery, which can be uncomfortable for the patient and increases the measurement time for the PET scan. For DV_t estimation, Logan introduced additional assumptions.[17] If k_2 can be given *a priori*, and if the existence of a receptor poor region, a reference region, can be assumed, $C_p(t)$ is canceled in (1). Moreover, if the equilibrium state between $C(t)$ and $C_p(t)$ is achieved, k_2 is unnecessary. A practical issue for Logan's approach is that k_2 is difficult to specify without knowledge about the behavior of the administered radioligand. Also, k_2 is uncommon in tissues, and it is laborious to obtain the values for every voxel or target region. Naganawa developed a new statistical information separation algorithm of EPICA to study the adenosine A_1[18] and A_{2A}[9]. EPICA does not require any assumptions of the kinetics of radioligands.[(1)]

Second, variations of the Logan plot are available. The Ogden plot[13] has been mentioned earlier. Ichise proposed a variation of the original Logan plot,[19] which assumes the existence of a reference region in which $C_p(t)$ is not required for the computation. The algorithms related to the Logan plot are compared in Ichise's study.[20]

Last, a starting time for the Logan plot should be considered. As mentioned in §II, the Logan plot is applicable if some equilibrium conditions are established. Accordingly, the starting time should be determined carefully. Some details of this are discussed by Ichise.[20]

VIII. CONCLUSION

Although the Logan plot is a routine tool for PET functional imaging, additional studies are still required. The Logan plot is easy to use, but thorough understanding of the algorithm is needed to utilize fully the information in measured PET data. We believe that the Logan plot has widespread applicability for quantitative imaging with PET in various clinical and physiological fields.

[(1)] The topics on the omission of arterial blood sampling will be discussed in more detail later in this survey series.

APPENDIX A

Derivation of Logan plot in matrix form

The Logan plot is applicable for both two- and three-compartment models, thus its derivation begins with a matrix fashion, and the operational equations for each

model are presented.

The measured PET data, $C(t)$, are the sum of the radioactivity concentrations in free and specific binding compartments, which are denoted as $C_f^{\sim}(t)$ and $C_b^{\sim}(t)$, respectively. Considering contribution from vessels in a voxel or ROI, $C(t)$ is written as:

$$C(t) = (1 - B_v)C^{\sim}(t) + B_v C_p(t) \quad \text{(A.1)}$$
$$C^{\sim}(t) = C_f^{\sim}(t) + C_b^{\sim}(t) \quad \text{(A.2)}$$

where B_v is the blood volume [m*l*/m*l*], and $C^{\sim}(t)$ is the total radioactivity concentration in a tissue. In a strict sense, $C_p(t)$ in (A.1) should denote the radioactivity in whole blood. In the following mathematical handling, $C_p(t)$ is assumed to be equal to that in whole blood. This assumption causes bias in the Logan plot when the metabolite is not small enough to ignore.

The differential equation to describe a compartmental model is:

$$\frac{dA}{dt} = KA(t) + C_p(t)Q. \quad \text{(A.3)}$$

For the two-compartment model, the equation is:

$$A(t) \triangleq C^{\sim}(t),\ K \triangleq -k_2,\ Q \triangleq K_1, \quad \text{(A.4)}$$

and for the three-compartment model, the equation is:

$$\begin{cases} A(t) \triangleq \begin{bmatrix} C_f^{\sim}(t) & C_b^{\sim}(t) \end{bmatrix}^T \\ K \triangleq \begin{bmatrix} -(k_2 + k_3) & k_4 \\ k_3 & -k_4 \end{bmatrix} \\ Q \triangleq \begin{bmatrix} K_1 & 0 \end{bmatrix}^T. \end{cases} \quad \text{(A.5)}$$

Here, ^{T} means a matrix transposition. To calculate $C^{\sim}(t)$, a new vector of U is defined:

$$U \triangleq \begin{cases} 1 & \text{for the two-compartment model} \\ \begin{bmatrix} 1 \\ 1 \end{bmatrix} & \text{for the three-compartment model} \end{cases} \quad \text{(A.6)}$$

and then $C^{\sim}(t)$ can be represented as $U^T A(t)$.

The Logan plot starts to be derived by integrating (A.3), and K^{-1} is premultiplied on both sides, which gives:

$$\int_0^t A(u)du = -K^{-1}Q\int_0^t C_p(u)du + K^{-1}A(t). \quad \text{(A.7)}$$

Here, no activities exist at the beginning of the PET scan, *e.g.* $A(0) = 0$. Next, the integral of $C^{\sim}(t)$ can be represented using (A.6):

$$\begin{aligned} \int_0^t C^{\sim}(u)du &= U^T \int_0^t A(u)du \\ &= -U^T K^{-1} Q \int_0^t C_p(u)du + U^T K^{-1} A(t). \end{aligned} \quad \text{(A.8)}$$

However, $C^{\sim}(t)$ is free from the activity originating from blood vessels and is not measurable. Using (A.1), an integrated measured tTAC is written as:

$$\begin{aligned} \int_0^t C(u)du &= (1 - B_v)\int_0^t C^{\sim}(u)du + B_v \int_0^t C_p(u)du \\ &= (1 - B_v)\left(-U^T K^{-1} Q \int_0^t C_p(u)du + U^T K^{-1} A(t)\right) \\ &\quad + B_v \int_0^t C_p(u)du \\ &= \left\{(1 - B_v)(-U^T K^{-1} Q) + B_v\right\}\int_0^t C_p(u)du \\ &\quad + (1 - B_v)U^T K^{-1} A(t). \end{aligned} \quad \text{(A.9)}$$

If both sides are divided by $C(t)$, a matrix form of the Logan plot is derived:

$$\begin{aligned} \underbrace{\frac{\int_0^t C(u)du}{C(t)}}_{Y} &= \left\{(1 - B_v)(-U^T K^{-1} Q) + B_v\right\} \underbrace{\frac{\int_0^t C_p(u)du}{C(t)}}_{X} \\ &\quad + (1 - B_v)\frac{U^T K^{-1} A(t)}{C(t)} \\ &\triangleq \alpha X + \beta. \end{aligned} \quad \text{(A.10)}$$

(A.10) denotes a linear relation between the X and Y if β is constant against time, a condition where the Logan plot is established.

APPENDIX B

Logan plot for the two-compartment model

From (A.4) and (A.10), for a two-compartment model, the slope is written as:

$$\alpha_{2C} = (1 - B_v)\frac{K_1}{k_2} + B_v. \quad \text{(B.1)}$$

If $B_v \neq 0$, the slope of the Logan plot corresponds to K_1/k_2, which is a distribution volume. The y-intercept is:

$$\begin{aligned} \beta_{2C} &= (1 - B_v)\frac{1\left(-\frac{1}{k_2}\right)C^{\sim}(t)}{C(t)} = -(1 - B_v)\frac{C^{\sim}(t)}{k_2 C(t)} \\ &= -\frac{1 - B_v}{k_2}\frac{C^{\sim}(t)}{(1 - B_v)C^{\sim}(t) + B_v C_p(t)}. \end{aligned} \quad \text{(B.2)}$$

By dividing the numerator and the denominator by $C^{\sim}(t)$:

$$\beta_{2C} = -\frac{1 - B_v}{k_2}\frac{1}{(1 - B_v) + B_v\frac{C_p(t)}{C^{\sim}(t)}} \quad \text{(B.3)}$$

can be derived. (B.3) indicates that the Logan plot is established if $C_p(t)/C^{\sim}(t)$ becomes constant against t.

APPENDIX C

Logan plot for three-compartment model

For a three-compartment model, the slope is:

$$\begin{aligned} \alpha_{3C} &= -\frac{1 - B_v}{k_2 k_4}\begin{bmatrix} 1 & 1 \end{bmatrix}\begin{bmatrix} -k_4 & -k_4 \\ -k_3 & -(k_2 + k_3) \end{bmatrix}\begin{bmatrix} K_1 \\ 0 \end{bmatrix} + B_v \\ &= (1 - B_v)\frac{K_1}{k_2}\left(1 + \frac{k_3}{k_4}\right) + B_v. \end{aligned} \quad \text{(C.1)}$$

If $B_v = 0$, the slope corresponds to the total distribution volume of a three-compartment model of $(K_1/k_2)(1 + k_3/k_4)$.

The condition to establish the Logan plot for a threecompartment model is rather complicated. From (A.5) and (A.10):

$$\beta_{3C} = (1 - B_v)\frac{\frac{1}{k_2k_4}[1 \;\; 1]\begin{bmatrix} -k_4 & -k_4 \\ -k_3 & -(k_2 + k_3) \end{bmatrix}\begin{bmatrix} \tilde{C_f}(t) \\ \tilde{C_b}(t) \end{bmatrix}}{C(t)}$$

$$= -\frac{1 - B_v}{k_2k_4}\left\{(k_3 + k_4)\frac{\tilde{C(t)}}{C(t)} + k_2\frac{\tilde{C_b}(t)}{C(t)}\right\}. \qquad \text{(C.2)}$$

Therefore, if $\tilde{C(t)}/C(t)$ and $\tilde{C_b}(t)/C(t)$ are constant against time, the y-intercept becomes constant, and the Logan plot is appropriate for the three-compartment model.

REFERENCES

1. Watabe H, Ikoma Y, Kimura Y, Naganawa M, Shidahara M. PET kinetic analysis—compartmental model. *Ann Nucl Med* 2006; 20 (9): 583–588.
2. Bard Y. The initial guess. In *Nonlinear Parameter Estimation*; chapter 5–20. Academic Press, Inc., 1974: 120–123.
3. Logan J, Fowler JS, Volkow ND, Wolf AP, Dewey SL, Schlyer DJ, et al. Graphical analysis of reversible radioligand binding from time-activity measurements applied to [*N*-^{11}C-methyl]-(–)-Cocaine PET studies in human subjects. *J Cereb Blood Flow Metab* 1990; 10 (10): 740–747.
4. Press WH, Teukolsky SA, Vetterling WT, Flannery BP. Fitting data to a straight line. In *Numerical Recipies in C, Second Edition*; chapter 15.2. Cambridge University Press, 1992: 661–666.
5. Mintun MA, Raichle ME, Kilbourn MR, Wooten GF, Welch MJ. A quantative model for the *in vivo* assessment of drug binding sites with positron emission tomography. *Ann Neurol* 1984; 15 (3): 217–227.
6. Koeppe RA, Holthoff VA, Frey KA, Kilbourn MR, Kuhl DE. Compartmental analysis of [^{11}C]Flumazenil kinetics for the estimation of ligand transport rate and receptor distribution using positron emission tomography. *J Cereb Blood Flow Metab* 1991; 11 (5): 735–744.
7. Marquardt DW. An algorithm for least-square estimation of nonlinear parameters. *J Soc Indust Appl Math* 1963; 11 (2): 431–441.
8. Nelder LA, Mead R. A simplex method for function minimization. *Computer J* 1965; 7: 308–313.
9. Naganawa M, Kimura Y, Mishina M, Manabe Y, Chihara K, Oda K, et al. Quantification of adenosine A_{2A} receptors in the human brain using [^{11}C]TMSX and positron emission tomography. *Eur J Nucl Med Mol Imaging* 2006. DOI: 10.1007/s00259-006-0294-0.
10. Ishiwata K, Tsukada H, Kawamura K, Kimura Y, Nishiyama S, Kobayashi T, et al. Mapping of CNS sigma$_1$ receptors in the conscious monkey: Preliminary PET study with [^{11}C]SA4503. *Synapse* 2001; 40: 235–237.
11. Logan J. Graphical analysis of PET data applied to reversible and irreversible tracers. *Nucl Med Biol* 2000; 27: 661–670.
12. Varga J, Szabo Z. Modified regression model for the Logan plot. *J Cereb Blood Flow Metab* 2002; 22: 240–244.
13. Ogden RT. Estimation of kinetic parameters in graphical analysis of PET imaging data. *Stat Med* 2003; 22: 2557–2568.
14. Drapper NR, Smith H. Straight line regression when both variables are subject to error. In *Applied regression analysis*; chapter 3.4. third edition. John Wiley & Sons, Inc., 1998: 89–96.
15. Slifstein M, Laruelle M. Effects of statistical noise on graphic analysis of PET neuroreceptor studies. *J Nucl Med* 2000; 41: 2083–2088.
16. Sakata M, Kimura Y, Naganawa M, Oda K, Ishii K, Chihara K, et al. Mapping of human cerebral sigma$_1$ receptors using positron emission tomography and [^{11}C]SA4503. *NeuroImage* 2006. DOI:10.1016/j.neuroimage.2006.11.055.
17. Logan J, Fowler JS, Volkow ND, Wang GJ, Ding YS, Alexoff DL. Distribution volume ratios without blood sampling from graphical analysis of PET data. *J Cereb Blood Flow Metab* 1996; 16 (5): 834–840.
18. Naganawa M, Kimura Y, Nariai T, Ishii K, Oda K, Manabe Y, et al. Omission of serial arterial blood sampling in neuroreceptor imaging with independent component analysis. *NeuroImage* 2005; 26 (3): 885–890.
19. Ichise M, Liow JS, Lu JQ, Takano A, Model K, Toyama H, et al. Linearized reference tissue parametric imaging methods: application to [^{11}C]DASB positron emission tomography studies of the serotonin transporter in human brain. *J Cereb Blood Flow Metab* 2003; 23: 1096–1112.
20. Ichise M, Toyama H, Innis RB, Carson RE. Strategies to improve neuroreceptor parameter estimation by linear regression analysis. *J Cereb Blood Flow Metab* 2002; 22: 1271–1281.